Efficient Structural Optimization of Aircraft Wings

Tiago Freire
tiago.a.freire@ist.utl.pt

Instituto Superior Técnico, Lisboa, Portugal

February 2017

Abstract

Nowadays, gradient-based methods are one of the most widely used tools in aircraft Multidisciplinary Design Optimization. However, these methods require the computation of the sensitivities of the interest functions with respect to the design variables, representing one of the most computationally expensive steps in the optimization process, since these are frequently obtained by approximation methods that are highly dependent on the number of design variables. Therefore, the main objective of this work is to develop an efficient optimization tool for wing preliminary design, using exact gradient information. Firstly, a survey on the existent sensitivity analysis methods is conducted, with the application to a beam design problem modeled with finite elements, providing valuable insight in the implementation process and advantages of each method. Subsequently, a tool to represent a 3D wing structure is adapted into three blocks and the correspondent modules for sensitivity computation are developed, with the application of the automatic differentiation, the symbolic derivative and the adjoint methods. A parametric study is presented for a reference wing case and the total sensitivities are computed with the developed framework and verified with the finite difference method. Lastly, structural optimization tests, using the reference case as the initial design point, are performed. The objective of minimizing the wing mass is achieved with a remarkable increase in computational efficiency in the optimization process, translated in a reduction of the computational time to, roughly, half and one third, when compared to the forward and central difference methods, respectively.

Keywords: Structural optimization, Gradient-based methods, Sensitivity analysis, Adjoint method, Automatic differentiation, Finite element method

1. Introduction

Over the past century, a remarkable progress in the history of aviation was observed and many different configurations of aircraft were developed. The aeronautical market is experiencing a growing trend and, in the next 15 years, the air traffic is expected to double. Therefore new aircraft need to be introduced with more efficient technology.

In order to improve global aircraft design, several disciplines must be simultaneously taken into account as a coupled Multidisciplinary Design Optimization (MDO) problem, using mathematical models dependent on a set of parameters that characterize a certain design. By varying these parameters, different concepts are generated and the main goal is to establish a compromise among the disciplines to generate better concepts. According to Sobieszczanski [1], there has been a rising interest in MDO applications in aerospace systems, but many challenges still exist concerning computational expense and organizational complexity. One of the possible solutions to accelerate optimization processes is to use gradient-based algorithms with highly efficient sensitivity computation methods, in order to lead the optimizer to an optimum design point, fast and accurately. The adjoint method is a good example of an efficient approach for gradient calculation, being the computational time practically independent on the number of design variables, and has been topic of research in many areas such as wing structural design, aerodynamic drag reduction, composite manufacturing and aero-structural problems.

Almeida [2] developed an aeroelastic tool that included a static aero-structural mode, which was used to perform test optimizations to minimize the wing's total mass for a given baseline configuration. Even though an optimal solution was obtained, the optimization was proven to be quite inefficient since the forward finite difference method was used to estimate the gradient information, requiring the evaluation of the entire aero-structural code multiple times per iteration.

The main objective of this work is to develop an efficient optimization tool for the structural problem in the aero-structural framework, relying on gradient-based information to find the best solution. An adjoint structural solver must be included in this framework and other alternative sensitivity analysis methods must be studied and compared. The sensitivity framework must be validated and tested for wing optimization cases.

2. Optimization Methods

Optimization can be defined as the act of obtaining the best result under given circumstances, and has a direct application in engineering problems. According to Belegundu [3], most engineering optimization problems can be mathematically expressed as non-linear programming (NLP) problems,

$$\begin{array}{lll} \text{minimize} & f_{obj}(\mathbf{x}) & \\ \text{w.r.t} & \mathbf{x} \in \mathbb{R}^n & \\ \text{subject to} & g_j(\mathbf{x}) \leq 0 \ , & j = 1, ..., \ell \\ \text{and} & h_k(\mathbf{x}) = 0 \ , & k = 1, ..., m \\ \text{and} & \mathbf{x}^L \leq \mathbf{x} \leq \mathbf{x}^U , & \end{array} \tag{1}$$

where $f_{obj}(\mathbf{x})$ is the objective function, which corresponds to a criterion for evaluating different designs dependent on the design vector $\mathbf{x} = (x_1, x_2, ..., x_n)^T$ of n design variables, which is limited by lower and upper bound vectors $\mathbf{x}^L$ and $\mathbf{x}^U$, respectively. The optimization problem is subjected to ℓ inequality constraints, $g_j(\mathbf{x})$, and to m equality constraints, $h_k(\mathbf{x})$. The term feasible design is used to describe a set of design variables that satisfies the constraints. In general, these problems can be divided in either gradient-based or gradient-free methods, depending on, whether or not, information on the derivatives of the objective and constraint functions is required.

Gradient-based methods are applied in design problems which have smooth objective functions and constraints, using gradient information to find an optimal solution. Most of the gradient-based algorithms comprise two subproblems:

1. Establishing the search direction.
2. Minimizing along that direction (or one-dimensional line search).

The main advantages of these methods are the rapid convergence to the optimum solution by exploiting gradient information and the possibility to establish a clear convergence criterion, assuring that the step size is under a certain order of magnitude and allowing local optimum identification. The main disadvantages include failing when noisy or discontinuous objective functions are considered and also tending to find a local optimum instead of guaranteeing a global optimum. Furthermore, the solution may be influenced by the initial design point choice, since different starting points may lead to different search directions.

The necessary optimality conditions can be derived for the nonlinear constrained optimization problems, based on the definition of the Lagrangian function ($\mathcal{L}$):

$$\mathcal{L}(\mathbf{x}, \lambda) = f(\mathbf{x}) + \sum_{j=1}^{l} \mu_j g_j(\mathbf{x}) + \sum_{k=1}^{m} \lambda_k h_k(\mathbf{x}) \ , \tag{2}$$

where λ_k and $\mu_j \geq 0$, are Lagrange multipliers defined for each constraint $h_k = 0$ and $g_j \leq 0$, respectively. It is assumed that f_{obj}, h_k and g_j are continuously differentiable over $\mathbb{R}^n$. If $\mathbf{x}^*$ is an optimal solution of the optimization problem, then there exist Lagrange multipliers μ^* and λ^* that satisfy the Karush-Kuhn-Tucker (KKT) optimality conditions:

$$\nabla_x \mathcal{L} = 0 \Rightarrow \frac{\partial \mathcal{L}}{\partial \mathbf{x}} = \frac{\partial f}{\partial \mathbf{x}} + \sum_{j=1}^{l} \mu_j \frac{\partial g_j}{\partial \mathbf{x}} + \sum_{k=1}^{m} \lambda_k \frac{\partial h_k}{\partial \mathbf{x}} = 0 \tag{3a}$$

$$g_j \leq 0, \quad i = 1, ..., \ell \tag{3b}$$

$$h_k = 0, \quad j = 1, ..., m \tag{3c}$$

$$\mu_j \geq 0, \quad i = 1, ..., \ell \tag{3d}$$

$$\mu_j g_j = 0, \quad i = 1, ..., m \ . \tag{3e}$$

Some examples of gradient-based methods that rely on these conditions are the Gradient Projection Method, the Feasible Directions Method or The Sequential Quadratic Programming (SQP).

Gradient-free methods are optimization approaches that do not require derivative information to find a solution and are based solely on the value of the objective function. An advantage in gradient-free methods the non requirement of a strong set of assumptions or global properties on the optimization problem and no necessity in calculating sensitivity information. Besides that, several algorithms are able to solve discrete optimization problems, usually tolerate noise in the objective function and are able to find a global optimum, instead of a local optimum. The main disadvantages concern the sensitivity to the dimension of the problems, increasing the computational cost due to the need of evaluating the objective function multiple times. It may also be difficult to establish an ending criterion. An example of gradient-free algorithms are the so-called "population based" algorithms, which engage a set of solutions (instead of a single solution) that are updated at every iteration, simulating the evolution or behavior of a population. Some examples of population based methods are: Genetic Algorithms, Particle Swarm Optimization and Ant Colony Methods.

Based on the overview of gradient-based and gradient-free methods presented, it is necessary to select one of the approaches to be applied to the structural framework. Since a highly efficient optimization is required, a high convergence speed method with clear convergence criteria seems to be the best choice. Furthermore, the structural model to be used is well established and the parameters to be treated as design variables are considered to be continuous. Methods that are dependent on the dimension of the problem shall be avoided, since if a high number of design variables is chosen, the optimization process will require a high number of evaluations to determine an optimum design. For all the reasons stated above, gradient-based methods will be used in this thesis. Note that in theory, these methods do not depend directly on the dimension of the problem. However, the method used to compute the sensitivities may (or not) be dependent on the number of design variables.

3. Sensitivity Analysis

Design sensitivity analysis consists in the computation of the dependence of an interest function (f), which can be either an objective function or a constraint, with respect to the design variables (x) and is considered one of the most computational expensive steps in the gradient-based optimization process. Sensitivity analysis methods can be divided in approximation and analytic methods. The former include finite difference and complex step methods which yield approximate result of the interest function's sensitivity. The latter exploits differential calculus concepts, such as symbolic differentiation and the chain rule, to obtain the true sensitivity values, being only affected by computational errors.

3.1. Symbolic Differentiation

The first analytical method to evaluate the sensitivity of a function is the symbolic differentiation. A function f is said to be differentiable with respect to x, if the following limit exists:

$$\frac{\mathrm{d}f}{\mathrm{d}x} \equiv \lim_{\Delta x \to 0} \frac{f(x+\Delta x) - f(x)}{\Delta x} \quad . \tag{4}$$

The limit represented in Equation (4) is known for several functions, allowing an explicit derivation of the function's sensitivity. Nevertheless, it is restricted to explicit functions and may become computationally expensive or even impracticable to calculate in high dimensionality problems.

3.2. Finite Difference Method

The finite difference method allows sensitivity estimation by approximating the derivative of a function with a quotient of differences and can be derived from a Taylor series expansion. The forward finite difference expression, whose truncation error is $\mathcal{O}(\Delta x)$, is given by

$$\frac{\mathrm{d}f}{\mathrm{d}x} = \frac{f(x+\Delta x) - f(x)}{\Delta x} + \mathcal{O}(\Delta x). \tag{5}$$

If a second-order estimation is desired, the central-difference formula may be used:

$$\frac{\mathrm{d}f}{\mathrm{d}x} = \frac{f(x+\Delta x) - f(x-\Delta x)}{2\,\Delta x} + \mathcal{O}[(\Delta x)^2]. \tag{6}$$

The main advantages in finite difference methods is the simplicity in implementation. However, for the multivariable case, it may become computationally expensive if many design variables are involved. Furthermore, there is the need to choose a small step-size to minimize truncation error, but at the same time guaranteeing that subtractive cancellation errors do not become dominant, making the task of choosing a design perturbation step-size a challenge.

3.3. Complex Step Method

The complex step method [4] uses a complex step perturbation $i\Delta x$ to calculate the sensitivity of an interest function, arising as a solution to overcome the problem of subtractive cancellation in the finite difference methods and leading to accurate and robust results. The sensitivity expression is calculated as

$$\frac{\mathrm{d}f(x)}{\mathrm{d}x} = \frac{\mathrm{Im}[f(x+i\Delta x)]}{\Delta x} + \mathcal{O}[(\Delta x)^2], \tag{7}$$

where $\mathcal{O}[(\Delta x)^2]$ represents the second-order truncation error. As in the finite difference case, the cost of estimating a sensitivity is directly proportional to the number of design variables n, becoming a disadvantage in using this method for problems with a great number of design variables. Furthermore, it may increase the computational cost and may be necessary to redefine some functions in the computer language to allow complex arguments.

3.4. Alternative Analytic Methods

According to Martins [5], alternative analytic approaches such as the adjoint and direct methods are the most efficient and accurate in sensitivity analysis. However, these methods require previous knowledge on the governing equations, which is a drawback when compared to other sensitivity analysis methods. For a general physical system, the governing equations can be represented in residual form,

$$\mathcal{R}(x_n, y_i(x_n)) = 0 \ , \tag{8}$$

where x_n is the design vector and y_i is the state variable vector. Using the chain rule to capture both explicit and implicit contributions of x_n, it is obtained:

$$\frac{\mathrm{d}\,f}{\mathrm{d}\,x_n} = \frac{\partial\,f}{\partial\,x_n} + \frac{\partial\,f}{\partial\,y_i}\frac{\mathrm{d}\,y_i}{\mathrm{d}\,x_n} \ , \tag{9}$$

where the partial derivative terms are given by differentiating the explicit terms in the interest function's expression. In order to solve the second term on the right-hand side, two approaches are found: the direct and the adjoint sensitivity methods.

3.4.1 Direct Sensitivity Method

The first approach to evaluate a function of interest's sensitivity corresponds to the direct method. Since the governing Equation (8) must always be satisfied, it is a necessary condition that the total derivative of the residuals with respect to any design variable is always equal to zero, meaning that

$$\frac{\partial \mathcal{R}}{\partial y_i}\frac{\mathrm{d}\, y_i}{\mathrm{d}\, x_n} = -\frac{\partial \mathcal{R}}{\partial x_n} \ . \tag{10}$$

Using Equation (10), the total derivative of the state variables with respect to design variables ($\frac{\mathrm{d}\, y_i}{\mathrm{d} x_n}$) is directly obtained and all the necessary information to solve Equation (9) is supplied.

Note that, by using the direct sensitivity method, Equation (10) has to be solved n times due to the term on the right hand side. Thus, the computational cost of using the direct method will depend considerably on the number of design variables.

3.4.2 Adjoint Sensitivity Method

The second approach to evaluate a function of interest's sensitivity uses the adjoint formulation. Combining Equations (9) and (10), results

$$\frac{\mathrm{d} f}{\mathrm{d}\, x_n} = \frac{\partial f}{\partial x_n} - \underbrace{\frac{\partial f}{\partial y_i}\left[\frac{\partial \mathcal{R}}{\partial y_i}\right]^{-1}}_{\psi^T}\frac{\partial \mathcal{R}}{\partial x_n} \ . \tag{11}$$

An auxiliary adjoint vector ψ is defined and can be determined by solving the adjoint equation:

$$\left[\frac{\partial \mathcal{R}}{\partial y_i}\right]^T \psi = \left[\frac{\partial f}{\partial y_i}\right]^T \ . \tag{12}$$

Note that, with this method, the calculation of the adjoint vector is independent on the number of design variables, depending only on the number of interest functions, and the total sensitivity with respect to the design can be evaluated with a small additional computational cost. Thus, this method is preferable if the number of design variables exceeds the number of interest functions.

3.5. Automatic Differentiation

Automatic differentiation [6] is an exact method that calculates sensitivities by applying the differentiation chain rule of Calculus systematically throughout the computer code, at elementary functions levels. This approach avoids approximation errors that exist in the finite difference method, and can be generated automatically, without the need of hand-coding, representing an advantage with respect to the alternative analytic methods. If major modifications need to be performed in the main program, a new updated version of the derivative computation is generated quickly. According to Berland [7], the procedure to implement an automatic differentiation algorithm comprises three steps:

1. Identify the intrinsic functions, based on the original source code;
2. Evaluate the derivatives of intrinsic functions;
3. Use the chain rule to obtain the desired derivative.

Any program may be decomposed into m elementary functions T_i, with $i = 1, ..., m$, and $t_i = T_i(t_1, ..., t_{i-1})$ correspond to the elementary variables. The chain rule of differentiation for a generic $\frac{\partial t_i}{\partial t_j}$ can be written as

$$\frac{\partial t_i}{\partial t_j} = \delta_{ij} + \sum_{k=j}^{i-1} \frac{\partial T_i}{\partial t_k}\frac{\partial t_k}{\partial t_j} \ , \tag{13}$$

where δ_{ij} is the Kronecker delta. Two modes may be used to propagate the derivatives throughout the chain rule: the forward mode, in which the bottom index j is chosen and kept fixed, varying the index i from j until the desired derivative (ultimately to m), or the reverse mode, in which the i index is fixed, varying the index j, in a descendant order, from i until the desired quantity (ultimately down to 1). One sweep of forward mode, determines one column vector of the Jacobian matrix and one sweep on the reverse mode calculates one row vector, meaning that the reverse mode is desirable if there are more variables than functions, and the forward mode is best suited if the number of functions is greater than the number of variables. However, the reverse mode requires more memory since the code is run once forward, storing all the intermediate variables, and once backward to apply the backwards chain rule.

The implementation of the forward automatic differentiation can be performed either by source code transformation, in which the original source code is analyzed, parsed and code associated with the derivative calculation is added; or by operator overloading, in which operators are redefined for dual numbers, being the first part of the number associated to the function's value and the dual part of the number containing the derivative information. The former approach will be used in this work with a tool called *ADiMat*.[8]

3.6. Benchmark

As a first approach to the implementation of sensitivity analysis methods to structural problems, a rectangular cantilevered Euler-Bernoulli beam with constant width b and heights h_1 and h_2 on the first and second halves of its length L was considered with a point load (P) applied at the tip, as represented in Figure 1.

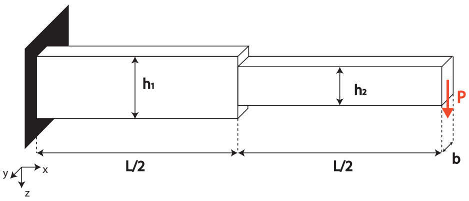

Figure 1: Cantilevered beam representation.

To describe the structural behavior of the beam, the Finite Element Method (FEM) [9] was chosen, which is a numerical method that is used to solve real world problems with complex physics, geometry and boundary conditions by dividing the overall problem's domain in many subdomains, and approximating the solution of the governing equation within each subdomain with simplified functions.

After developing the finite element code, a reference beam was chosen with $b = 25$mm, $h_1 = 35$mm, $h_2 = 30$mm, corresponding to the design variables (x_n), and $P = 100N$ and $L = 2$m. The Young's modulus of the material used was $E = 70\times$ GPa. Two functions of interest are considered: the vertical tip displacement (f_1) and the bending moment at the built in end (f_2). The latter function is only used to verify code implementation, since the moment applied at the root is independent of the design variables, yielding a zero sensitivity.

The sensitivities were computed with the forward difference (FD) and central difference (CD) methods, by using Equations (5) and (6); the complex method (CM), by using Equation (7); the forward algorithmic differentiation, by using *ADiMat* and the alternative analytical methods (direct and adjoint). The last two used the direct equation,

$$K_{ki}\,\frac{\mathrm{d}\,y_i}{\mathrm{d}\,x_n} = -\frac{\partial\,K_{ki}}{\partial\,x_n}\,\tilde{y_i}\;, \tag{14}$$

and the adjoint equation,

$$K_{ik}\,\psi_k = \frac{\partial f}{\partial y_i}\;, \tag{15}$$

respectively, where K_{ki} represents the reduced stiffness matrix, $\tilde{y_i}$ the solution for the considered design point and ψ_k, the adjoint vector. The sensitivities obtained with the adjoint method were used as reference. According to Table 1, it is observable that an increase of b, h_1 or h_2, leads to a decrease in the tip deflection (f_1), since the sensitivity values are negative for the three cases, being the h_1 the variable with the highest influence. The sensitivities relative to f_2 were omitted since these were verified to be approximately zero.

In Figure 2, the relative error of the tip displacement sensitivity with respect to the beam cross-sectional width is presented in a logarithmic scale.

Sensitivity	$\frac{\mathrm{d}f_1}{\mathrm{d}b}$ [-]	$\frac{\mathrm{d}f_1}{\mathrm{d}h_1}$ [-]	$\frac{\mathrm{d}f_1}{\mathrm{d}h_2}$ [-]
Value	-1.83134E-05	-3.19867E-05	-8.46561E-06

Table 1: Sensitivity analysis results with the adjoint method.

For the FD, linear convergence is verified and a relative optimum step of 2.5×10^{-8} is observed. For the CD quadratic convergence is obtained and a relative optimum step of 7.94×10^{-6} is verified. For the CM quadratic convergence is observed and the error converges for steps lower than 10^{-9}. For the optimal steps, CM presented the lowest sensitivity errors, followed by CD and FD.

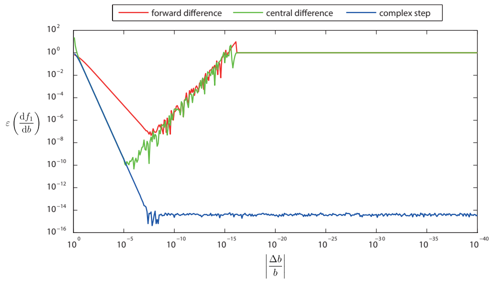

Figure 2: Logarithmic plot of $\varepsilon(\frac{\mathrm{d}f_1}{\mathrm{d}b})$ as a function of the relative step size.

For the values of the sensitivities obtained it was verified that FD and CD presented relative errors in the order of 10^{-8} and 10^{-10}, respectively, for optimal steps. For the complex step, automatic differentiation, direct and adjoint methods similar sensitivities were obtained, with relative errors in the order of 10^{-14}. Thus, the method to be used in the wing structural problem must result from a trade-off between the complexity in implementing and execution time.

4. Structural Framework

In order to assess the structural behavior of a 3D aircraft wing, a framework was developed comprising the following three modules: the equivalent cross-sectional properties; the equivalent beam element properties; and the finite element model.

4.1. Equivalent cross-sectional properties

The first module determines the cross-sectional properties at a certain position along the wing span, using a thin-wall wingbox approximation model (Figure 3) and will be utilized to evaluate the cross-sectional properties at the nodes locations.

The inputs of each cross-section are the chord length (c), the front and rear spars location $(x_1/c$, $x_2/c)$, the wingbox segment's thicknesses $(t_A$, t_B, t_C and $t_D)$, the Young's modulus (E) and the material density (ρ). The outputs correspond to the

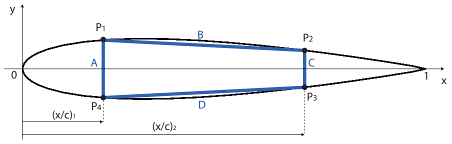

Figure 3: Thin-wall wingbox approximation of a NACA0015 airfoil, in the airfoil's reference frame.

shear center location (SC_x, SC_y), the axial stiffness EA, the bending stiffnesses EI_{xx} and EI_{yy}, and torsional rigidity GJ. The steps to obtain these properties are the following:

- Characterize the airfoil and generate the wingbox based on the input parameters;
- Determine the centroidal axis and compute the moments of area contributions of each wingbox segment relative to the centroid;
- Calculate the shear center location, corresponding to the point where shear loads produce no twist;
- Determine axial and bending stiffness relative to the shear center;
- Compute the torsional stiffness with the Bradt-Batho Shear Flow Theory;
- Calculate the linear density (ρ_l) of the cross-section.

4.2. Equivalent Beam Element Properties

The second module performs a weighted average of the structural properties between two sections of the wing, and will be used to determine each beam element's properties. The inputs correspond to the structural properties (EA, EI_{xx}, EI_{yy}, GJ and ρ_l) at the boundaries (nodes). The outputs are the average area (A_{av}), average moments of inertia (I_{av}) and average polar moment of inertia (J_{av}), which are calculated as

$$A_{\text{av}} = \frac{A_1 + \sqrt{A_1\,A_2} + A_2}{3} \,, \tag{16a}$$

$$I_{\text{av}} = \frac{I_1 + \sqrt[4]{I_1^3\,I_2} + \sqrt{I_1\,I_2} + \sqrt[4]{I_1\,I_2^3} + I_2}{5} \,. \tag{16b}$$

The expression for J_{av} is the same as in Equation (16b). The indexes 1 and 2, correspond to the properties on the limits of the considered element. The average linear density ($\rho_{l_{av}}$) is also obtained as an output and is simply given by the arithmetic mean value at the boundaries.

4.3. Finite Element Model

The third module generates the finite element model of the wing and evaluates its structural response to an aerodynamic loading. The low fidelity 3D beam finite element (Figure 4) is chosen since it allows fast generation of concepts in preliminary design stages and assesses important structural responses. This corresponds to a unidimensional finite element model, delimited by two nodes with six degrees of freedom each: three displacement components (u_x, u_y, u_z) and three rotation components (θ_x, θ_y, θ_z).

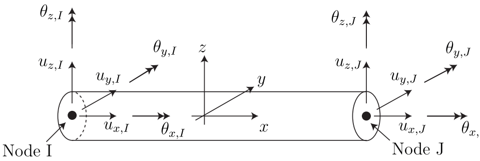

Figure 4: 3D-beam element representation.

This general beam element results from the conjugation of an axial bar element, two bending beam elements and a torsion bar element, whose governing equations are given, respectively, by:

$$\frac{d}{dx}\left(EA\frac{du_x}{dx}\right) + b(x) = 0 \,, \tag{17}$$

$$\frac{d^2}{dx^2}\left(EI_{yy/zz}\frac{d^2u_{z/y}}{dx^2}\right) - q(x) = 0 \,, \tag{18}$$

$$\frac{d}{dx}\left(GJ\frac{d\theta_x}{dx}\right) + m(x) = 0 \,. \tag{19}$$

The variables EA, EI and GJ represent axial, bending and torsional rigidity, respectively, and the variables $b(x)$, $q(x)$ and $m(x)$ correspond to distributed axial, bending and twisting loads.

In order to formulate the stiffness matrix, it is necessary to establish the shape function and organize them in a matrix $[N]$. The axial displacement (u_x) and torsion (θ_x) are modeled with linear shape functions and for the transverse displacements (u_y and u_z), cubic shape functions along x were utilized. The full displacement field for a 3D beam element can be determined using

$$\mathbf{u} = [N]\,\mathbf{y} \,, \tag{20}$$

where $\mathbf{u}$ is the vector of displacements and $\mathbf{y}$ is the vector of nodal displacements.

The derivation of the stiffness matrix can be performed by using the concept of potential energy [2]. For a general finite element, the potential energy can be defined as

$$\begin{aligned} V =& \frac{1}{2}\mathbf{y}^T\int_\Omega [B]^T\,[D]\,[B]\,\mathrm{d}\Omega - \mathbf{y}^T\int_\Omega [N]^T\,\mathbf{f_v}^T\mathrm{d}\Omega \\ & - \mathbf{y}^T\int_S [N]^T\,\mathbf{f_s}^T\mathrm{d}S \,. \end{aligned} \tag{21}$$

where Ω corresponds to the element domain, S to the element's surface, $\mathbf{f_v}$ to the volume forces and $\mathbf{f_s}$ to the surface forces. In this case, the stress vector, the elasticity matrix and the strain vector are slightly modified, to represent the axial force, bending moment in both planes and the torsional moment, as

$$\begin{Bmatrix} N_x \\ M_z \\ M_y \\ M_x \end{Bmatrix} = \begin{bmatrix} EA & 0 & 0 & 0 \\ 0 & EI_{zz} & 0 & 0 \\ 0 & 0 & EI_{yy} & 0 \\ 0 & 0 & 0 & GJ \end{bmatrix} \begin{Bmatrix} \epsilon_x(x) \\ \kappa_z(x) \\ \kappa_y(x) \\ \theta_(x) \end{Bmatrix} = [D]\,\boldsymbol{\epsilon} \; . \tag{22}$$

Note that the modified strain vector includes the axial strain, curvatures and twist angle. The modified strain-displacement relation is given by

$$\boldsymbol{\epsilon} = [B]\;\mathbf{y} = \begin{bmatrix} \frac{\partial}{\partial x} & 0 & 0 & 0 \\ 0 & \frac{\partial^2}{\partial x^2} & 0 & 0 \\ 0 & 0 & \frac{\partial^2}{\partial x^2} & 0 \\ 0 & 0 & 0 & \frac{\partial}{\partial x^2} \end{bmatrix} [N]\;\mathbf{y} \; . \tag{23}$$

The stiffness matrix of the element is identified from Equation (21) and is computed as

$$[K^e_\ell] = \int_\Omega [B]^T [D][B] d\Omega \; . \tag{24}$$

In general, the local reference frame of the finite element is different from the global frame and it may be useful to represent the results in the global frame. The relation between the element coordinates and the global coordinates is given by

$$\mathbf{y}_\ell = [T^e]\,\mathbf{y} \; , \tag{25}$$

where $\mathbf{y}_\ell$ corresponds to the vector of displacements in the element Cartesian coordinates and $\mathbf{y}$ represents the vector of displacements in the global Cartesian coordinates. The element stiffness matrix in the global reference frame ($[K^e]$) may be calculated as

$$[K^e] = [T_R]^T \left[K^e_\ell\right] [T_R] \; . \tag{26}$$

After defining the element stiffness matrices in the global reference frame and assemble the global matrix, it is necessary to determine the global force vector containing the aerodynamic information to be applied at the nodes of the beam finite elements. The aerodynamic analysis is performed by using an incompressible potential flow panel method code developed in MATLAB®. The pressures are assumed to be constant within each panel and the resultant forces applied at each panel's collocation point may be estimated by multiplying the area of each panel by the dynamic pressure $0.5\rho V_\infty^2$, where ρ represents the density of the fluid and V_∞ the free stream velocity. To transfer the forces in the panels to the structural nodes, each collocation point force ($\mathbf{f_i}$) is decomposed into the respective global reference frame components, and the equivalent moments relative to the structural node are calculated using an auxiliary orientation vector ($\mathbf{r_i}$) defined from the structural point to the considered collocation point as

$$\mathbf{m_i} = \mathbf{r_i} \times \mathbf{f_i} \; . \tag{27}$$

Note that the collocation points are located in the same cross-sectional plane as the structural nodes to simplify load transfer.

Having the global stiffness matrix and force vector, the reduced system of equations shall be obtained from applying the essential boundary conditions. The wing is modeled as a clamped beam, meaning that the first six degrees of freedom are fixed corresponding to the node of the first element, that is located at the wing root section. Thus, the reduced stiffness matrix is obtained by eliminating the first six rows and columns from the global stiffness matrix. The corresponding first six entries of the external force vector are removed, as well. Hence, all the conditions required to obtain the static structural solution of the problem are fulfilled.

5. Structural Framework

After defining the structural framework, parametric studies were carried out to verify how output functions are influenced by changing some parameters from the baseline configuration. Only internal geometric parameters and material properties will be considered in these studies. The external shape is not changed, in order to obtain a constant external aerodynamic loading. The baseline external and internal wing geometries, the material properties and the flight condition are summarized in Table 2.

External Geometric Parameters		**Internal Geometric Parameters**	
Half-wing spanwise length (L)	7 m	Front spar location (x_1/c)	0.25
Root chord (c_{root})	1 m	Rear spar location (x_2/c)	0.75
Angle of attack (α)	2°	Front spar thickness (t_A)	20 mm
Sweep (Λ)	0°	Upper skin thickness (t_B)	5 mm
Dihedral (Γ)	0°	Front spar thickness (t_C)	20 mm
Taper ratio (λ)	1	Lower skin thickness (t_D)	5 mm
Twist at the tip (ϑ_{tip})	0°		
Material Properties		**Flight Condition**	
Density (ρ)	2800 kg/m^3	Altitude (h)	1370 m
Young's modulus (E)	75 GPa	Air density (ρ_{air})	1 kg/m^3
Shear modulus (G)	30 GPa	Freestream velocity (V_∞)	75 m/s

Table 2: Reference wing baseline parameters.

Four interest functions are considered in this parametric study: the total wing mass (m_{wing}), which is given by the sum of the linear density times the length of each finite element and is often desired to be minimized in aircraft design, to achieve better performance; the wing tip vertical displacement (δ_{tip}), which is directly obtained from the finite element solution vector $\mathbf{y}$ and may be used as a constraint to assure that the tip displacement does not surpass a predefined maximum allowable value; the tip rotation (θ_{tip}), which is also obtained directly from $\mathbf{y}$ and may be used as a constraint; and the maximum stress at the wing root, which only considers the direct axial stress plus the absolute values of both axial stress components originated from bending as

$$\sigma_x = \frac{N_x}{A} + \frac{M_z d_y}{I_{zz}} + \frac{M_y d_z}{I_{yy}} \ , \qquad (28)$$

where d_y corresponds to the distance from the shear center to the considered spar, and d_z corresponds to half the length of that spar. Since there are two spars in this wingbox model, Equation (28) has to be evaluated twice for a corner point of each spar. Afterwards, it must be checked which of the two cases presents the highest stress value to be defined as the maximum axial stress (σ_{max}).

The influence of the spars' location along the airfoil is the first case that is assessed, as represented in Figure 5. A specific example is presented in Figure 6, where it is observable that the total mass of the wing decreases when moving the front spar (A) in the rear direction. This occurs because an increase in x_1/c leads to a reduction of the upper and lower wingbox segment's lengths. Thus, the linear density of the cross-section will be lower than in the reference case, since there is less material per cross-section segment, resulting in an overall mass reduction. The reverse happens when moving the rear spar (C) in the rearwards direction.

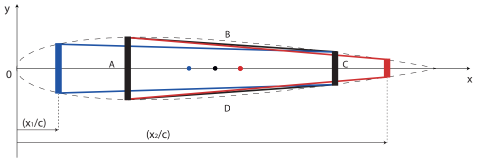

Figure 5: Wing box configurations by changing the spars locations.

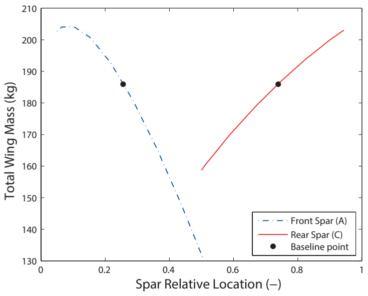

Figure 6: Influence of the spars locations in the wing mass.

The thickness of the wingbox segments (Figure 7) is also considered in the parametric studies. An example is illustrated in Figure 8, where it is verified that an increase of the thickness of any section of the wingbox leads to a decrease in the vertical tip displacement. This occurs due to an increase in bending stiffness. Out of the three cases presented in Figure 8, the thickness of the front spar has the greatest impact in the vertical tip displacement.

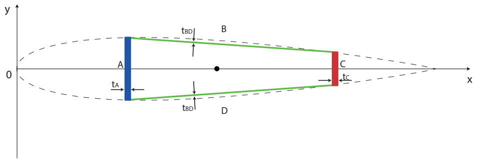

Figure 7: Representation of the thicknesses of the wingbox segments.

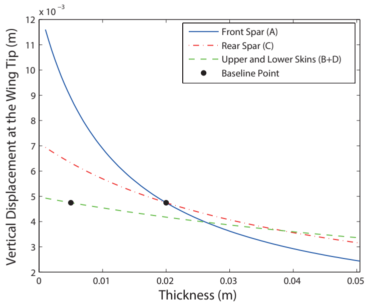

Figure 8: Influence of the wingbox segment's thickness in the tip vertical displacement and rotation.

Similar tests performed for the material properties including the material density, the Young's modulus and the shear modulus.

The results obtained with the parametric study are summarized in Table 3. Note that "$\searrow$" corresponds to a decrease in the output function with an increase in the variable's value. Similarly, "$\nearrow$" represents an increase and "$-$" means that no influence is verified. These results are valid in the neighborhood of the baseline point.

Increase in	m_{wing}	δ_{tip}	θ_{tip}	σ_{max}
Front spar location (x_1/c)	$\searrow$	$\searrow$	$\nearrow$	$\nearrow$
Rear spar location (x_2/c)	$\nearrow$	$\nearrow$	$\nearrow$	$\nearrow$
Front spar thickness (t_A)	$\nearrow$	$\searrow$	$\searrow$	$\searrow$
Skin thickness (t_{BD})	$\nearrow$	$\searrow$	$\searrow$	$\searrow$
Rear spar thickness (t_C)	$\nearrow$	$\searrow$	$\nearrow$	$\searrow$
Density (ρ)	$\nearrow$	-	-	-
Young's modulus (E)	-	$\searrow$	-	-
Shear modulus (G)	-	-	$\searrow$	-

Table 3: Effect of the parameters studied on the output functions.

6. Sensitivity Analysis Framework

After evaluating how the parameters influence the output functions, three auxiliary modules are introduced in the framework to compute the exact derivative information: the automatic differentiation, the explicit derivative and the adjoint method, represented in dashed boxes in Figure 9. The design vector $\mathbf{d}$ corresponds to a vector of dimension

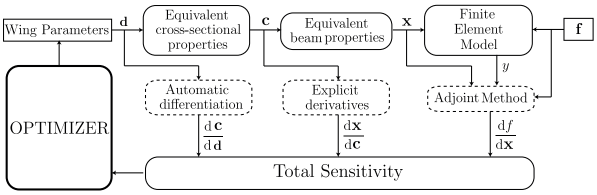
Wing Parameters
d
Equivalent cross-sectional properties
c
Equivalent beam properties
x
Finite Element Model
f
y
OPTIMIZER
Automatic differentiation
Explicit derivatives
Adjoint Method
$\frac{\mathrm{d}\mathbf{c}}{\mathrm{d}\mathbf{d}}$
$\frac{\mathrm{d}\mathbf{x}}{\mathrm{d}\mathbf{c}}$
$\frac{\mathrm{d}f}{\mathrm{d}\mathbf{x}}$
Total Sensitivity

Figure 9: Structural optimization framework.

$5\,(n_{fe}+1)$, where n_{fe} represents the number of finite elements, containing the parametrized internal structure configuration at each node location, being organized as

$$\mathbf{d} = [x_1/c \; x_2/c \; t_A \; t_{BD} \; t_C]_i^T \;, \tag{29}$$

with $i = 1, ..., n_{fe}+1$.

The cross-section properties information vector $\mathbf{c}$ represents a vector of dimension $6(n_{fe}+1)$ containing the cross-section properties at the nodes locations, calculated in the shear center frame, as well as the shear center chordwise coordinate, represented in the airfoil frame, being written as

$$\mathbf{c} = \mathbf{c_1} \cup \mathbf{c_2} \cup \mathbf{c_3} = [EA_c \, EI_{zz_c} \, EI_{yy_c} \, GJ_c]_i^T \cup [SC_{x_c}]_i \cup [\rho_{l_C}]_i \;, \tag{30}$$

where $\mathbf{c_1}$, $\mathbf{c_2}$ and $\mathbf{c_3}$ represent segments of the vector $\mathbf{c}$.

The vector $\mathbf{x}$, of dimension $6\,n_{fe}$, contains the average material properties of each finite element and the shear center location at the end node of the finite element (SC_x) as

$$\mathbf{x} = \mathbf{x_1} \cup \mathbf{x_2} \cup \mathbf{x_3} = [EA \, EI_{zz} \, EI_{yy} \, GJ]_j^T \cup [SC_{x_c}]_j \cup [\rho_l]_j \;, \tag{31}$$

with $j = 1, ..., n_{fe}$

For a general interest function f, the calculation of its sensitivity with respect to the design variables can be written as

$$\frac{\mathrm{d}f}{\mathrm{d}\mathbf{d}} = \frac{\mathrm{d}f}{\mathrm{d}\mathbf{x}} \cdot \frac{\mathrm{d}\mathbf{x}}{\mathrm{d}\mathbf{c}} \cdot \frac{\mathrm{d}\mathbf{c}}{\mathrm{d}\mathbf{d}} \;, \tag{32}$$

where:

- $\frac{\mathrm{d}\mathbf{c}}{\mathrm{d}\mathbf{d}}$ is computed with automatic differentiation;
- $\frac{\mathrm{d}\mathbf{x}}{\mathrm{d}\mathbf{c}}$ is obtained by using explicit differentiation;
- $\frac{\mathrm{d}f}{\mathrm{d}\mathbf{x}}$ is found by applying the adjoint method.

Note that for each module, the most suitable exact method was chosen. For the first module, symbolic differentiation was not applicable due to the complexity of the problem and the alternative analytic sensitivity were not suitable since the finite element solution is not involved in this part of the program, leaving the automatic differentiation as the only possible approach. For the second module, the explicit expressions were available and due to their low complexity symbolic differentiation was a suitable approach. For the third module, the adjoint method was chosen, being the most efficient exact method available, since the number of intermediate design variables (x) was greater than the number of interest functions dependent on the structural solution. The first and third methods were validated with the forward finite difference method. The second method required no benchmark due to its simplicity of implementation.

Also notice that, depending on the interest function f, it may not be necessary to run all the modules in the optimization chain.

If the cross-sectional geometric configuration are forced to be equal at every cross-section, the total sensitivity is obtained by summing the contributions of each individual cross-section $\mathbf{d_i}$. Thus a new design vector $(\mathbf{v})$ is defined as

$$\mathbf{v} = [x_1/c \;\; x_2/c \;\; t_A \;\; t_{BD} \;\; t_C]^T \;. \tag{33}$$

The total sensitivity results are presented in Table 4. The signs of the sensitivities may be verified with the qualitative analysis performed in Table 3. This may also be confirmed by analyzing the slopes of the lines tangent to the curves at the baseline points represented in the parametric studies figures: the sign of the slope corresponds to the sign of the correspondent sensitivity. Also, the higher the magnitude of the derivative, the steeper the slope of the line tangent to the curve at the baseline point.

v	$\frac{\mathrm{d}m_{wing}}{\mathrm{d}v}$	$\frac{\mathrm{d}\delta_{tip}}{\mathrm{d}v}$	$\frac{\mathrm{d}\theta_{tip}}{\mathrm{d}v}$	$\frac{\mathrm{d}\sigma_{max}}{\mathrm{d}v}$
x_1/c	-1.7140E+02	-1.0187E-03	5.7000E-03	4.7191E+05
x_2/c	9.0828E+01	5.3706E-03	2.1334E-03	2.4783E+06
t_A	2.8943E+03	-1.4764E-01	-2.3479E-02	-7.1689E+07
t_{BD}	1.9646E+04	-4.3310E-02	-2.4537E-01	-2.8343E+07
t_C	1.5475E+03	-7.8937E-02	1.4222E-02	-3.7224E+07

Table 4: Sensitivity of the interest functions with respect to the geometrical wing parameters.

The respective verification of the total sensitivity analysis framework was performed with the forward finite difference method. The results of the relative errors obtained for the finite difference case, using the total sensitivity calculated with this framework as reference, shown relative differences smaller than 0.0143%, proving the correct implementation of the framework.

7. Wing Structural Optimization

The final stage of this project corresponds to use the sensitivity analysis framework in a structural optimization problem of an aircraft wing. The function `fmincon` from MATLAB® Optimization Toolbox was used to solve nonlinear constrained multivariable optimization problems, using the Sequential Quadratic Programing algorithm. The optimization problem is given by Equation (34) where the objective is to minimize wing mass, with a set of constraints in the vertical tip displacement, tip rotation and maximum stress at the root. The initial design and respective upper and lower bounds are described in Table 5.

$$\begin{aligned} \underset{\mathbf{v}}{\text{minimize}} \quad & m_{wing}(\mathbf{v}) \\ \text{subject to} \quad & \delta_{tip}(\mathbf{v}) - 0.05\text{m} \leq 0 \ , \\ & \theta_{tip}(\mathbf{v}) - 1^\circ \leq 0 \ , \\ & \sigma_{max}(\mathbf{v}) - 322\text{GPa} \leq 0 \ , \\ & \mathbf{v}^L \leq \mathbf{v} \leq \mathbf{v}^U \end{aligned} \tag{34}$$

Design vector ($\mathbf{v}$)	Initial design ($\mathbf{v_0}$)	Lower bound ($\mathbf{v^L}$)	Upper bound ($\mathbf{v^U}$)
x_1/c [-]	0.25	0.20	0.40
x_2/c [-]	0.75	0.60	0.80
t_A [mm]	20.00	1.00	30.00
t_{BD} [mm]	5.00	1.00	8.00
t_C [mm]	20.00	1.00	30.00

Table 5: Inital values and bounds of the design variables.

The initial and final results in the optimization problems are summarized in Table 6. It can be observed that the wing mass decreased from 187.006 kg to 16.795 kg. The vertical tip displacement and tip rotation have tended to the upper limits of the constraint, being equal to the defined maximum values. The maximum stress falls below the maximum stress limit. In the new wing configuration, the rear spar was moved to the lower bound and the front spar was shifted towards the trailing edge. All the specified thicknesses decreased and the skin thickness was equal to the lower bound.

Design variables	Initial	Optimized	Output functions	Initial	Optimized
x_1/c [-]	0.25	0.3856	m_{wing} [kg]	187.066	16.795
x_2/c [-]	0.75	0.60	δ_{tip} [mm]	4.748	50.000
t_A [mm]	20	2.1199	θ_{tip} [°]	0.0809	1.000
t_{BD} [mm]	5	1	σ_{max} [Pa]	2.320E+06	2.38634E+07
t_C [mm]	20	1.0324			

Table 6: Initial and optimized results.

The results obtained using the sensitivity framework were benchmarked with the forward and central finite difference methods (Table 7). The optimal configurations were the same in the three cases, however, the sensitivity framework was proven to be the most efficient, requiring almost half of the time when compared to the forward finite difference and roughly one third of the time when compared to the central finite difference.

Gradient calculation method	Time [s]	No. iterations	Function evaluations
Sensitivity framework	16.58	9	10
Forward finite difference	28.21	9	60
Central finite difference	46.78	9	110

Table 7: Excecution time, iterations and function evaluations for three different sensitivity calculation methods.

8. Conclusions

With this work, an efficient optimization tool for wing structural design was developed, relying on gradient-based information to find the best solution. The most expensive step found in these methods, concerning the sensitivity computation with the usage of approximation methods that are highly dependent on the number of design variables, was overcome by developing an exact sensitivity analysis framework comprising the algorithmic differentiation, the explicit differentiation and the adjoint methods. Ultimately this framework was linked to an optimizer and structural optimization examples demonstrated not only convergence to better designs, in terms of objective function values, but also improvements in terms of efficiency, clearly noticeable with the reduction of the computational time for almost half, when using the forward finite differences, and for roughly a third, when using the central differences.

References

[1] J. Sobieszczanski-Sobieski and R. T. Haftka. Multidisciplinary aerospace design optimization: survey of recent developments. *Structural Optimization*, 14(1):1–23, 1997.

[2] João Almeida. Structural dynamics for aeroelastic analysis. Master's thesis, Técnico Lisboa, October 2015.

[3] Ashok D. Belegundu. *Optimization Concepts and Applications in Engineering*. Cambridge University Press, 2^{nd} edition, 2011.

[4] J. N. Lyness. Numerical algorithms based on the theory of complex variable. In *Proceedings of the 22nd ACM National Meeting*, 1967.

[5] Joaquim R. R. A. Martins. *A Coupled-Adjoint Method for High Fidelity Aero-structural Optimization*. PhD thesis, Stanford University, October 2002.

[6] Christian Bischof, Paul Hovland, and Boyana Norris. On the implementation of automatic differentiation tools. *Higher-Order and Symbolic Computation*, 21(3):311–331, 2008.

[7] Hårvard Berland. Automatic differentiation. Department of Mathematical Sciences, NTNU, September 2006.

[8] H. Martin Bücker. Combining source transformation and operator overloading techniques to compute derivatives for MATLAB programs. IEEE Computer Society.

[9] J.N. Reddy. *An Introduction to the Finite Element Method*. McGraw-Hill Education, 3rd edition, 2005.